Revision 2

Influence of temperature and Cl on the hydrothermal replacement of calcite by apatite and the development of porous microstructures

Laura Jonas*, Timm John, and Andrew Putnis

Institut für Mineralogie, Westfälische Wilhelms-Universität Münster, Corrensstrasse 24, D-48149 Münster, Germany

* Present address: Institut für Geologie, Mineralogie und Geophysik, Ruhr-Universität Bochum, Universitätsstrasse 150, D-44801 Bochum, Germany

E-mail: Laura.Jonas@ruhr-uni-bochum.de

Abstract

Calcite ($CaCO_3$) powder was replaced by hydroxylapatite [$Ca_5(PO_4)_3OH$] in hydrothermal experiments at temperatures between 120 °C and 180 °C, and times between two and twelve hours, in 1.0 *M* $(NH_4)_2HPO_4$ solutions. Additional experiments using concentrations of up to 2.0 *M* NH_4Cl as an additional component were carried out to examine the influence of Cl on the process. X-ray powder diffraction and Rietveld refinements were used to determine the proportion of parent and product phases after each experiment. The resultant data on the fraction transformed as a function of temperature and time were plotted according to the Avrami equation and an activation energy of 118 kJ/mol was determined for the replacement process without Cl in solution, whereas with 0.5 – 2.0 *M* Cl in solution, the activation energy varied from 131 kJ/mol to 145 kJ/mol. No simple correlation between the chlorinity of the solution and the value of the activation energy was observed. However, the

data indicates that the mechanism controlling the reaction changes between 140 °C and 160 °C, correlating with systematic differences in abundance, size, and geometry of the porosity in the apatite formed in the replacement process. At lower temperature, the pores are small and oriented parallel to the reaction interface, whereas at higher temperature, the pores are larger and orientated perpendicular to the interface. Changes in the porosity during the replacement process make it problematic to determine a meaningful value for the activation energy for such replacement processes, since the mechanism controlling the reaction depends on factors other than the temperature, such as the availability and form of the pathways allowing the fluid to reach the unreacted core of the single crystals.

Keywords: apatite, hydrothermal replacement, kinetic data, reaction mechanisms, activation energy

Introduction

Due to its ability to incorporate a large variety of different cations and anions, apatite [$Ca_5(PO_4)_3(OH,F,Cl)$] plays an important role in aqueous solution-solid solution interactions as well as in fluid-rock interactions and hydrothermal processes (e.g. Ayers and Watson 1993; Brenan 1993; Engvik et al., 2009; Kasioptas et al. 2011). For example, the incorporation of halogens such as F and Cl into the apatite structure makes apatite a useful indicator for interpreting halogen contents and activities in various geological environments, since Cl and F are important constituents of hydrothermal fluids (e.g. Brenan 1993; Kullerud et al. 2001; Patiño Douce and Roden, 2006). Brenan (1993) examined the partitioning of Cl and F between apatite and aqueous fluids at high temperature and pressure. His results indicate that amounts of Cl and F incorporated into coexisting apatite depend on the fluid composition as well as on the absolute abundances of chlorine and fluorine in the fluid.

The interaction of phosphate-bearing fluids with carbonates is relevant in a wide range of geological and industrial situations. For example, understanding the kinetics of the

precipitation of calcium phosphate phases like apatite is of great importance for treating ground- and waste-waters (Larsen and Pearce 2002). Larsen and Pearce (2002) showed that boiling a suspension of brushite [$CaHPO_4 \cdot 2H_2O$] and calcite rapidly converts the two salts to well-crystallized apatite. Because this well-crystallized apatite incorporates fluoride if present in solution, the authors proposed that the above process may be exploited to remove excess fluoride from drinking water. Wang et al. (2012) used atomic force microscopy (AFM) to study the interaction of phosphate-bearing solutions with calcite surfaces. They showed that adsorption of phosphate and corresponding precipitation of calcium orthophosphate phases such as hydroxylapatite on the calcite surface decreases the concentration of dissolved phosphate in soil solution and thus its bioavailability. Solution additives such as salts may even further decrease the concentration of phosphate in solution. The addition of citrate to the phosphate solution on the other hand suppressed the formation of calcium orthophosphates on the calcite surface. Thus the study by Wang et al. (2012) showed that understanding the kinetics of calcium orthophosphate dissolution and precipitation has possible implications for the management of phosphate dissolution and precipitation in soils. Sassoni et al. (2011) observed that hydroxylapatite formed by the reaction of limestone with a solution of diammonium hydrogen phosphate at room temperature appears to be a promising consolidant to protect carbonate stones from weathering. They demonstrated that such a treatment using a phosphate solution increases the mechanical properties of the samples, such as the dynamic strength modulus as well as the tensile strength.

The hydrothermal replacement of calcium carbonates by apatite has been subject of various studies in the past (e.g. Eysel and Roy, 1975; Yoshimura et al., 2004; Kasioptas et al., 2010, 2011), and is known to involve a coupled dissolution of the calcite and precipitation of porous apatite, preserving the morphology of the original calcite crystals. A previous study of the replacement (Kasioptas et al., 2010) suggested that the activation energy, the rate constant k, and the n values derived from fitting the data to an Avrami equation varied significantly as

a function of temperature and reaction progress. The focus of the present paper is to investigate the kinetics of the reaction in more detail and compare this to the evolution of the porous microstructure as a function of temperature as well as to determine the influence of chlorine concentration in solution on the activation energy.

Materials and methods

Calcite powder made from optically clear calcite crystals was used in this study. The crystals were cleaved using a razor blade, crushed using a mortar and sieved to obtain a grain size of 100-160 μm. The powder was ultrasonically cleaned to remove any finer particles. Additionally, larger crystals of a more-or-less rhombohedral shape and measuring ~1.8×2.2×2.6 mm were separated from a cleavage fragment using a razor blade.

To examine the influence of different concentrations of Cl on the replacement reaction, three stock solutions were prepared from $(NH_4)_2HPO_4$ powder (>99%, Acrōs Organics), NH_4Cl powder (99.8%, T.H. Geyer GmbH) and MilliQ water: 2.0 *M* $(NH_4)_2HPO_4$ and 2.0 *M* as well as 4.0 *M* NH_4Cl. Combining these stock solutions together with MilliQ water, five different solutions were prepared (Table 1). The pH of these solutions varied between ~8.1 and 7.6 with increasing chlorine concentration.

For each experiment calcite starting material was put into a Teflon©-lined autoclave together with 2.0 ml of liquid. The autoclaves were sealed, placed into a furnace and heated at different temperatures for different amounts of time. The pressure was not controlled as an additional factor. After being removed from the furnace, the autoclaves were cooled to room temperature using an electric fan for about five minutes. The pH of the reacted liquid was measured again after the reaction. The product powder was washed with distilled water and dried.

To determine the influence of temperature on the replacement reaction, each solution was reacted with ~90mg of calcite powder at four different temperatures from 120 °C to

180 °C for durations from 2 to 12 h (experiment set 1, Table 2). The products from these powder experiments were analyzed using X-ray powder diffraction. An X'Pert PW 3040 PANalytical diffractometer was used to identify the different phases using the X'Pert Data Collector software. The diffraction data was collected in the range 15 ° - 68 ° 2θ using $CuK\alpha_1$ radiation. The step size was 0.02 ° 2θ. The primary monochromator used was a Johannson monochromator with a Ge crystal cut on plane (111). The measurement time for each sample was 88 minutes. An initial analysis of the results was made with the X'Pert High Score and X'Pert Data Viewer. To determine the relative amounts of the different phases, a quantitative Rietveld analysis was carried out using the FullProf Suite (Rodriguez-Carvajal, 2001). Structural data like atom positions of the different mineral phases were taken from the literature (Graf 1961; Hughes et al. 1989; Yashima et al. 2003).

A further set of experiments was carried out using single crystals of calcite in order to examine the apatite reaction rims more closely. Experiments with varying amounts of Cl in solution (set 2), with varying reaction times (set 3) as well as experiments at different temperature (set 4) were carried out in order to study the amount of Cl incorporated into the apatite rim, the progress of the reaction rim towards the core of the crystals, and the microstructure of the reaction rim at different temperature levels (Table 2).

Mounted and polished cross-sections of the calcite crystals were examined by scanning electron microscopy (JEOL JSM-6610LV) and electron microprobe (JEOL JXA 8900 Superprobe) to determine both the microstructure and the composition of the apatite reaction rim.

Results

Both calcite ($CaCO_3$) and hydroxylapatite [$Ca_5(PO_4)_3OH$] were identified in each sample after the reaction. Additionally, β-tricalcium phosphate (β-TCP) [$Ca_3(PO_4)_2$] was found in some samples which were reacted at 160 °C for at least six hours or at 180 °C for

two to twelve hours. This form of TCP is known to be stable at temperatures below 1125 °C (Ryu et al. 2003). The amount of β-TCP varied between ~ 3 and 8 wt%; no clear trend as a function of temperature, duration or molarity could be observed. The amount of the apatite formed increases with temperature. After 12 h, most of the samples which reacted at 160 °C or 180 °C were almost completely transformed, containing ≥90 wt.% of apatite. At 120 °C and 140 °C, the amount of apatite formed in the same time is less than 50 wt%. The amount of apatite formed increases with the duration of the reaction (Fig. 1). A strong temperature dependence of the reaction rate can be observed in the increasing values for the rate constant *k* with increasing temperature for all reactions with varying chlorine concentrations in solution. At 120°C, *k* has very small values of 0.001-0.003, whereas at higher temperatures, *k* increases to up to 0.284-0.431 at 180°C (Table 3).

Figure 2 is a back-scattered electron (BSE) image of a typical result of the reaction carried out with single crystals of calcite at 200 °C with the progression of the reaction from the rim towards the core of the crystal. The developing reaction rim has a porous microstructure. Figure 2c shows an almost completely transformed single crystal with only a small calcite core remaining. The outer part of this crystal shows a slightly lower back-scattered intensity than the inner part around the small calcite core, with the two regions separated by an irregular interface. The crystal in Figure 2b also shows a similar variation in back-scattered intensity. Although no compositional difference between the two parts of the rim could be detected, high-magnification images show that the change in back-scattered intensity is related to a change in porosity (Fig. 2d). The two parts of the reaction rim showing different porous structures are separated by a sharp but irregular rather than straight interface (Fig. 2d). In the outer, darker colored part of the rim, the pores are larger and more elongate, forming channel-like structures (Fig. 3a). The length of these channel-like structures in the outer part of the rim varies between ~2.2μm and ~14.1μm. In the inner, lighter-colored part

(Fig. 3b), small pores with a pore diameter between ~0.1μm and ~0.3μm and some small pore-channels with a length between ~0.9μm and ~2.2μm can be observed.

In crystals that reacted at lower temperatures (140°C and 160°C for four days) there were also differences in the morphology of the porous microstructure (Fig. 4). At 140 °C (Fig. 4a), the pores in the reaction rim are relatively small and most of them have a clear prolate shape with a length between ~0.5μm and ~1.8μm . These pores are arranged in linear arrays orientated parallel to each other and the reaction interface. Though showing a variation in the size and length, the overall shape of the pores developed at 140°C is more or less uniform. At 160 °C (Fig. 4b), however, the pores are significantly larger and developed a more elongated shape. They even form channel-like structures with a length between ~9.2μm and ~52.6μm perpendicular to the reaction interface, directly penetrating the reaction rim towards the unreacted calcite core. In this case, the pores are still oriented more or less parallel to each other, but it is obvious that the pores do not have the common uniform shape that can be observed in the pores developed at 140°C. Although the general orientation of the channel-like pore structures is perpendicular to the interface, most show a certain tortuosity and are not as straight as the pores shown in Figure 4a.

In reactions containing Cl in solution there was no clear trend between the fraction transformed and the Cl-concentration. Electron microprobe data showed that the amount of Cl incorporated in the reaction rim of the larger calcite crystals increases as a function of the amount of Cl in solution (Fig. 5). However, no pure chlorapatite was formed.

The pH of the solutions slightly increased after the reaction. No significant difference was observed between the experiments with different Cl concentrations, except that the pH values for solutions with low Cl concentration were always slightly higher, both before and after the experiment. A slightly larger increase in pH was observed for the higher temperature runs. In general, the change in pH did not exceed 10%.

Kinetic data analysis

To determine the activation energy for the replacement process for different Cl-concentrations, we used the Avrami equation (Eq. 1)

$$y = 1 - e^{-(k \cdot t)^n} \quad (1)$$

where k is the rate constant, t is the duration of the experiment in hours, y is the fraction transformed to apatite, and n is the order of the reaction. The standard method is to transform this equation to:

$$-\ln\ln(1-y) = n \cdot \ln(k) + n \cdot \ln(t) \quad (2)$$

and plot the experimental data as -ln(ln(1-y)) against 1/T with T as the temperature in K. This plot should be linear with gradient n, and an intercept the y-axis of n·ln(k). The activation energy E_a can then be calculated by plotting ln(k) against 1/T according to the Arrhenius equation

$$k = A \cdot e^{\left(-\frac{Ea}{R} \cdot T\right)} \quad (3)$$

where A is the frequency factor and R the gas constant. A distinctive feature of the Avrami plots (Fig. 6) is that the gradients for the data collected at 120 °C and 140 °C are almost parallel while the gradients for 160 °C and 180 °C have a higher slope and are also almost parallel. Furthermore, there is a larger scatter of the data for the 160 °C and 180 °C experiments than for those at 120 °C and 140 °C. The calculated activation energies from these data are listed in Table 4.

Discussion

The mechanism and kinetics of the mineral replacement of calcium carbonate by apatite

Previous studies (e.g. Eysel and Roy 1975; Kasioptas et al. 2010, 2011) have shown that the replacement of calcite and aragonite by apatite is pseudomorphic and consistent with an interface-coupled dissolution-precipitation mechanism (Putnis and Putnis 2007; Putnis

2009) with the replacement taking place along an interface which migrates into the crystal from the surface of the carbonate. The progress of the replacement is dependent on the generation of porosity in the forming apatite allowing transport between the reaction interface and the fluid reservoir. This coupled dissolution and precipitation mechanism preserves the original morphology of the precursor phase, even when this is in the form of a finely structured biomaterial such as coral (Roy and Linnehan 1974; Xu et al. 2001; Hu et al. 2001) or cuttlebone (Kasioptas et al. 2010).

Although previous studies established a general relationship between the extent of the reaction and temperature, there have been few attempts to determine a value of the activation energy. In our experiments the amount of apatite formed as a function of time also increased at higher temperatures. At the lowest studied temperature of 120 °C, only ~ 17–20 wt% of calcite was transformed to apatite even after 12 h of reaction. Yoshimura et al. (2004) showed that at even lower temperatures of about 80 °C, no conversion to hydroxylapatite occurred in their experiments. Eysel and Roy (1975) replaced slices of aragonite crystals by hydroxylapatite at temperatures between 260 °C and 400 °C in hydrothermal experiments and also stated that the reaction proceeds slowly at lower temperatures.

Previous values of the activation energy for the replacement reaction of calcium carbonate by apatite have been determined for biogenic aragonite (as cuttlebone) by Kasioptas et al. (2010) who found that the activation energies varied with temperature as well as with the extent of the reaction, suggesting that the reaction controlling mechanism not only changed with temperature but also with time. Their values, determined using the same equation, average around 18.0 kJ/mol at temperatures between 80 °C and 100 °C and around 47.0 kJ/mol in the temperature range from 115 °C to 140 °C, considerably lower than the values found in our study. However, there is no reason to expect that the activation energy for aragonite replacement by apatite should be the same as that for calcite nor that single crystals of calcite should transform as readily as cuttlebone. Cuttlebone has a very open chamber-like

internal structure with horizontal septa and fine vertical pillars together with β-chitin as an additional component which makes up ~10 wt.% of the cuttlebone material. These differences in composition, size, and, especially, internal structure of the starting material may have led to different values for the activation energy.

Problems of determining activation energy for mineral replacement reactions

The determination of activation energy for mineral replacement reactions, as well as reactions generally termed "leaching" where a solid composition is changed by the interaction with a fluid, has been the subject of considerable discussion for some time. Although there is a general temperature dependence that would seem to justify the use of an Arrhenius equation from the extent of the reaction at different temperatures, the empirical activation energy determined from such an approach is not straightforward to interpret. As shown in Figure 2, the mechanism of the replacement reaction retains the morphology of the parent calcite crystal with a reaction front that moves progressively from the original calcite surface into the crystal interior. Such an interface-coupled dissolution-precipitation reaction mechanism is common in solid-fluid reequilibration processes (Putnis 2009). The individual reaction steps in the overall process involve the dissolution of the parent and the transport of the reactants to and from the reaction interface. The interpretation of the overall activation energy and the comparison of the present results with those of previous works must therefore bear in mind the factors that can affect these separate steps.

Comparison of the new results on the mechanisms and the activation energy for the replacement of calcite by apatite to those of Kasioptas et al. (2010) shows that changes in the reaction conditions such as the starting material, the reaction temperature, etc. may have great influence on the reaction controlling mechanism and may lead to changes in the values determined for the activation energy. Figure 7 summarizes some of the different factors that can affect the reaction rates and mechanisms. When a reaction involves so many steps each of

which is governed by a number of variables, the meaning of any determined activation energy is ambiguous. Thus, to discuss and compare the activation energies for different processes, similar experimental conditions are necessary. Additionally, it must be considered that different calculation approaches will lead to different activation energy values, even for the same process.

In our experiment we used $(NH_4)_2HPO_4$ solutions with added NH_4Cl to provide Cl. The empirical activation energy for the replacement of calcite by apatite in the presence of Cl in solution is significantly higher than in Cl-free solution, indicating that changes in the solution composition affect the rates. It is rarely possible to predict which step of the process is affected by fluid composition as the close coupling between dissolution and precipitation also means that the rates of the separate steps may not be very informative. The effect of fluid composition has also been demonstrated by Lemos et al. (2006) who produced carbonated hydroxylapatite from milled oyster shell powders (containing both aragonite and calcite) using a $(NH_4)_2HPO_4$ solution at 200 °C for different durations between 24 h and 92 h, adding various amounts of tetraethyl ammonium hydroxide (TENOH) and KH_2PO_4 to the solution. The TENOH increased the rate of transformation of calcite to apatite, but was less effective regarding the transformation of aragonite to apatite. An opposite effect was observed for solutions containing KH_2PO_4. Further, the use of these additives seemed to result in different preferred occupancies of the CO_3^{2-} ions within the crystal structure of apatite. Xu et al. (2001) showed that the conversion of the coral *Porites* into apatite involves a complex transformation process involving parallel reactions: one being the direct transformation of aragonite into hydroxylapatite, and a second, more complicated reaction, with intermediate conversions of aragonite to calcite, calcite to β-TCP, and β-TCP to hydroxylapatite. However, by adding the mineralizer KH_2PO_4, the conversion of aragonite to calcite and the formation of β-TCP was efficiently inhibited and the conversion of aragonite and apatite was consequently accelerated.

Such experiments highlight the fact that both the nature of the solid material to be replaced and the solution used for the hydrothermal replacement influence the reaction and its kinetics.

In our experiments the starting compositions are always undersaturated with respect to both calcite and apatite. The dissolution of calcite by the phosphate solution results in supersaturation with respect to apatite at the solid-fluid interface and not necessarily in the bulk solution, as evidenced by the fact that the replacement is pseudomorphic. However, it is not possible to determine the saturation state of the interfacial fluid in such experiments, nor do we know the relevant volume of the interfacial fluid which is supersaturated. The pseudomorphism suggests that it is the dissolution rate, rather than the precipitation rate which controls the kinetics. The dissolution rate is coupled to the interfacial fluid composition which in turn depends on the transport properties of the porous apatite product. These factors make a discussion of the mechanism much more complex than merely considering independent parameters that control dissolution and precipitation rates.

Another approach to analyzing so-called "leaching reactions" is to use the shrinking core model (e.g. Wen 1968; Pritzker 1996). Leaching reactions are, in terms of mechanism, equivalent to interface-coupled dissolution-precipitation reactions (Janssen et al., 2010). In the shrinking core model, the rate is controlled by the diffusion of material through a porous product phase, similar to that produced in our experiments. However, this approach could not be fitted to the data produced in our experiments.

The effect of fluid-pathway geometries on the activation energy

One aspect of the kinetics of interface-coupled dissolution-precipitation that has not been adequately addressed is the effect of fluid-pathway geometries on the overall kinetics and hence on the determined values of the activation energy. As noted above, the generation of porosity (and by implication the permeability) in the reacted rim is a prerequisite for a replacement reaction to proceed as it allows fluid transport and element exchange between the

reaction front and the fluid reservoir. The nature of this porosity (connectivity, tortuosity, pore size etc.) will therefore play a major role in determining the reaction rate. In the limiting case, a reaction rim with no porosity will completely armor the calcite from the reacting fluid.

The factors that determine the porosity in the product include the change in the molar volume between the parent and product solids as well as the relative solubility of the phases in the fluid. This latter factor determines the difference between the amount of parent dissolved and the amount of product precipitated. A model example has been determined in considerable detail for the case of single crystals of KBr pseudomorphically replaced by porous single crystals of KCl when reacted with a saturated KCl solution (Pollok et al. 2011). They determined the contribution of solubility to volume change and how this changes in a system where there is a solid solution between the parent and product and where the porosity changes with the extent of reaction. A study by Raufaste et al. (2011) on the same salt system revealed that the development of straight pores increases the rate at which the replacement front advances, allowing a maximum rate of solute transport. These pores are transient features as they disappear during annealing of the product phase after the replacement process stops and chemical gradients in the porosity filling fluid are equalizing (Raufaste et al. 2011). Although the KBr-KCl system is different from the present calcite-apatite system in that it involves a solid solution between two salts with much higher solubilities, we emphasize that it is the difference in solubility rather than the absolute solubilities that determine the porosity development (Pollok et al., 2011). Studies on simple salt systems indicate the importance of the development of a porous microstructure during replacement and the way in which chemical equilibration is accompanied by textural equilibration (Putnis et al., 2005). The evolution of the geometry of the pore system is likely to be a determining factor in the reaction rate.

In our study, we found significant changes in the geometry of the porosity between 140 °C and 160 °C as described above (Fig. 4). In contrast to the pores developed at 140 °C,

the porosity in the samples that reacted at 160 °C forms channel-like structures with a large diameter perpendicular to the reaction interface, allowing a more direct transport of solutes towards the inner part of the crystal. The same elongate pores can be found in the outer part of the reaction rim of an almost completely transformed calcite crystal that reacted at 200 °C for three days. In the inner part of the reaction rim, however, the pores remain relatively small, similar to the pore structures that developed at 140 °C after four days. It is likely that these changes in the morphology and porosity of the rim are reflected in the change in the determined activation energy between 140 °C and 160 °C, since changes in the pore geometry may change the rate of the reaction.

A further point which may be responsible for the variability in reaction rate is that the calcite crystals used in this study were crushed to a small grain size, and cracks and defects of different extent may have been introduced, providing additional pathways for the fluid and thus leading to a higher amount of fraction transformed. Partial replacement along fractures or, in general, the availability of all kinds of pathways for the fluid, is an important aspect controlling the amount of fraction transformed as well as the composition of the fluid at the reaction interface and the bulk fluid. Thus, the availability and geometry of fluid pathways will have an influence on the value of the activation energy calculated.

It should be noted that the intracrystalline porosity is itself a dynamic and transient feature. Ultimately, textural equilibration can result in coarsening and loss of connectivity, reducing the efficiency of mass transport and the overall reaction rate with time (Putnis et al. 2005; Raufaste et al. 2011).

The incorporation of Cl into hydroxylapatite

At the highest Cl concentrations in the fluid, the amount of Cl incorporated into the apatite was less than 0.8 wt% compared to ~ 7.0 wt% in pure chlorapatite. The reason that chlorapatite with Cl>OH did not form, can be understood from the relationship between the

crystal-melt partition coefficient and the effective ionic radii of halide anions in the apatite structure (Fig. 8). The preference for incorporating smaller ions is consistent with our observation that in the presence of both OH and Cl, the smaller OH ion will preferentially be incorporated over the larger Cl ion (Fig. 8). However, the almost linear increase of the amount of Cl incorporated in apatite as a function of the amount of Cl in solution (Fig. 5) confirms the results by Brenan (1993), who reacted natural fluorapatite with aqueous Na_2CO_3, NaOH, NaCl, HCl, and CO_2-H_2O mixtures at a pressure of 1.0-2.0 GPa and temperatures between 950 °C and 1050 °C. In his study, Brenan (1993) showed that, using fluid mixtures with a Cl content of up to 15 wt.%, the ratio X_{ClAp}/X_{OHAp} in apatite increases proportionally with the content of Cl in the fluid, with X_{ClAP} and X_{OHAP} representing the mole fractions of chlor- and hydroxylapatite.

Although the presence of Cl in solution leads to a general increase of the value of the activation energy for the hydrothermal replacement of calcite by apatite, no simple relationship between the value of the activation energy as a function of the chlorinity of the solution could be observed.

Concluding remarks

The data shows that our understanding of the kinetics of mineral replacement reactions and the influence of different factors that may determine the reaction mechanism is still incomplete. When Hancock and Sharp (1972) presented a concept for interpreting kinetic data, they already mentioned possible difficulties that might lead to problems in determining the exact kinetics of mineral reactions. The reaction mechanism may, as is the case here and as reported by Redfern (1987) and Kasioptas et al. (2010), change as a function of temperature. These authors also found that the reaction mechanism may also change after a certain fraction of the material has been transformed.

Among all possible factors that may influence the reaction mechanism and thus the activation energy (Fig. 7), the temperature and the availability of fluid pathways in the developing reaction front appear to be the most important factors controlling the replacement reaction examined in our study. Depending on the reaction temperature and duration, different porous structures develop, allowing a more-or-less direct transport of matter to and from the reaction interface. The relative rates of transport of carbonate and phosphate species through the fluid-filled intracrystalline porosity may also affect the overall reaction rate. The other factors mentioned above can be assumed to have an influence on the replacement reaction as well, albeit to a lesser extent than the temperature and the availability of fluid pathways.

Acknowledgements

The authors would like to thank Angelika Breit for XRD measurements, Dr. Peter Schmid-Beurmann for help with quantitative Rietveld analysis, Dr. Christine Putnis for help with scanning electron microscopy, and also the referees for their constructive comments. The Deutsche Forschungsgemeinschaft (DFG) financially supported this research through grant JO 349/3-1.

References cited

Ayers, J.C. and Watson, E.C. (1993) Apatite/fluid partitioning of rare-earth elements and strontium: Experimental results at 1.0 GPa and 1000 °C and application to models of fluid-rock interactions. Chemical Geology, 110, 299-314.

Brenan, J. C. (1993) Partitioning of fluorine and chlorine between apatite and aqueous fluids at high pressure and temperature: implications for the F and Cl content of high P-T fluids. Earth and Planetary Science Letters, 117, 251-263.

Dong, P. (2005) Halogen-element (F, Cl, and Br) behaviour in apatites, scapolite, and sodalite: An experimental investigation with field applications, 222p. Ph.D. thesis, University of Saskatchewan, Saskatoon, Canada.

Engvik, A.K., Golla-Schindler, U., Berndt, J., Austrheim, H., and Putnis, A. (2009) Intragranular replacement of chlorapatite by hydroxy-fluor-apatite during metasomatism. Lithos, 112, 236-246.

Eysel, W. and Roy, D.M. (1975) Topotactic reaction of aragonite to hydroxyapatite. Zeitschrift für Kristallographie, 141, 11-24.

Graf, D.L. (1961) Crystallographic tables for rhombohedral carbonates. American Mineralogist, 46, 1283-1316.

Hancock, J.D. and Sharp, J.H. (1972) Method of comparing solid-state kinetic data and its application to the decomposition of kaolinite, brucite, and $BaCO_3$. Journal of the American Ceramic Society, 55, 74-77.

Hu, J., Russell, J.J., and Ben-Nissan, B. (2001) Production and analysis of hydroxyapatite from Australian corals via hydrothermal processes. Journal of Materials Science Letters, 20, 85-87.

Hughes, J.M., Cameron, M., and Crowley, K.D. (1989) Structural variations in natural F, OH and Cl apatites. American Mineralogist, 74, 870-876.

Janssen, A., Putnis, A., Geisler, T., and Putnis, C.V. (2010) The experimental replacement of ilmenite by rutile in HCl solutions. Mineralogical Magazine, 74, 633-644.

Kasioptas, A., Geisler, T., Putnis, C.V., Perdikouri, C., and Putnis, A. (2010) Crystal growth of apatite by replacement of an aragonite precursor. Journal of Crystal Growth, 312 , 2431-2440.

Kasioptas, A., Geisler, T., Perdikouri, C., Trepmann, C., Gussone, N., and Putnis, A. (2011) Polycrystalline apatite synthesized by hydrothermal replacement of calcium carbonates. Geochimica et Cosmochimica Acta, 75, 3486-3500.

Kullerud, K., Flaat, K., and Davidsen, B. (2001) High-pressure fluid-rock reactions involving Cl-bearing fluids in lower-crustal ductile shear zones of the Flakstadøy Basic Complex, Lofoten, Norway. Journal of Petrology, 42, 1349-1372.

Larsen, M.J. and Pearce, E.I.F. (2002) Defluoridation of drinking water by boiling with brushite and calcite. Caries Research, 36, 341-346.

Lemos, A.F., Rocha, J.H.G., Quaresma, S.S.F., Kannan, S., Oktar, F.N., Agathopoulos, S., and Ferreira, J.M.F. (2006) Hydroxyapatite nano-powders produced hydrothermally from nacreous material. Journal of European Ceramic Society, 26, 3639-3646.

Patiño Douce, A.E. and Roden, M. (2006) Apatite as a probe of fugacities in the terrestrial planets. Geochimica et Cosmochimica Acta, 70, 3173-3196.

Pollok, K., Putnis, C.V., and Putnis, A. (2011) Mineral replacement reactions in solid solution-aqueous solution systems: Volume changes, reactions paths and end-points using the example of model salt systems. American Journal of Science, 311, 211-236.

Pritzker, M.D. (1996) Shrinking-core model for systems with facile heterogeneous and homogeneous reactions. Chemical Engineering Science, 51, 3631-3645.

Putnis, A. (2009) Mineral replacement reactions. Reviews in Mineralogy & Geochemistry, 70, 87-124.

Putnis, A. and Putnis, C.V. (2007) The mechanism of reequilibration of solids in the presence of a fluid phase. Journal of Solid State Chemistry, 180, 1738-1786.

Putnis, C.V., Tsukamoto, K., and Nashimura, Y. (2005) Direct observation for pseudomorphism: Compositional and textural evolution at a solid-fluid interface. American Mineralogist, 90, 1909-1912.

Raufaste, C., Jamtveit, B., John, T., Meakin, P., and Dysthe, D.K. (2011) The mechanism of porosity formation during solvent-mediated phase transformations. Proceedings of the Royal Society A, 467, 1408-1426.

Redfern, S.A.T. (1987) The kinetics of dehydroxylation of kaolinite. Clay Minerals, 22, 447-456.

Rodríguez-Carvajal, J. (2001) FullProf Suite. Laboratoire Léon Brillouin (CEA-CNRS), CEA/Saclay, 91191 Gif sur Yvette Cedcex, France.

Roy, D.M. and Linnehan, S.K. (1974) Hydroxyapatite formed from coral skeletal carbonate by hydrothermal exchange. Nature, 274, 220-222.

Ryu, H.-S., Hong, K.S., Lee, J.-K., Kim, D.J., Lee, J.H., Chang, B.-S., Lee, D.-h., Lee, C.-K., and Chung, S.-S. (2003): Magnesia-doped HA/β-TCP ceramics and evaluation of their biocompability. Biomaterials, 25, 393-401.

Sassoni, E., Naidu, S., and Scherer, G.W. (2011) The use of hydroxyapatite as a new inorganic consolidant for damaged carbonate stones. Journal of Cultural Heritage, 12, 346-355.

Wang, L., Ruiz-Agudo, E., Putnis, C.V., Menneken, M., and Putnis, A. (2012) Kinetics of calcium phosphate nucleation and growth on calcite: Implications for predicting the fate of dissolved phosphate species in alkaline soils. Environmental Science and Technology, 46, 834-842.

Wen, C.Y. (1968) Noncatalytic heterogeneous solid-fluid reaction models. Industrial and Chemical Engineering, 60, 34-54.

Xu, Y., Wang, D., Yang, L., and Tang, H. (2001) Hydrothermal conversion of coral into hydroxyapatite. Materials Characterization, 47, 83-87.

Yashima, M., Sakai, A., Kamiyama, T., and Hoshikawa, A. (2003) Crystal structure analysis of β-tricalcium phosphate $Ca_3(PO_4)_2$ by neutrin powder diffraction. Journal of Solid State Chemistry, 175, 272-277.

Yoshimura, M., Sujaridworakun, P., Koh, F., Fujiwara, T., Ponkao, D., and Ahniyaz, A. (2004) Hydrothermal conversion of calcite crystals to hydroxyapatite. Materials Science and Engineering C, 24, 521-525.

Figure Captions

Figure 1. Amount of apatite formed as a function of time at 120 °C (a), 140 °C (b), 160 °C(c) and 180 °C (d). In each plot, the black curve shows an example of the amount of apatite formed at a certain molarity including error bars for the calculated amount of apatite in wt%. All the data collected at other chlorine concentrations in solutions lie within the shaded areas.

Figure 2. BSE images showing the progress of the reaction rim (pale) towards the darker calcite core of the crystals that reacted at 200 °C with 1.0 *M* Cl in solution for different durations (a: one day; b: two days; c: three days). In the almost completely transformed crystal, the reaction front can be separated into an exterior and interior part with different porosity structures, resulting in different back-scattered intensities (d). Thus, the exterior part of the reaction rim is slightly darker than the interior part surrounding the unreacted calcite core. These two parts of the reaction front a separated by an irregular interface indicated by the dashed line in (d).

Figure 3. BSE-image showing the change of the porous microstructure of the reaction rim. In the outer part of the reaction rim (a), the pores are larger and have an elongated shape. In the inner part of the reaction rim close to the calcite core (b), the single pores are much smaller and not as elongated as in the exterior part.

Figure 4. Microstructure of the porous reaction rim of single crystals of calcite that reacted at 1.0 *M* Cl in solution for four days at 140 °C (a) and 160 °C (b). Note the different scale bars pointing out the significant difference in the pore size. Lighter colored spots close to pore structures are due to charging because of the high porosity of the reaction front preventing an even coating of the whole sample surface with carbon.

Figure 5. Amount of chlorine incorporated in the reaction rim (wt%) of single calcite crystals that reacted at 200 °C over a period of two days measured with the electron microprobe. The amount of Cl incorporated in apatite increases with increasing amount of Cl in solution.

Figure 6. Avrami plot of the data collected from experiments with no chlorine in solution and with 0.5-2.0 *M* Cl. The slope of the gradients increases between 140 °C and 160 °C and suggests a change in the mechanism controlling the reaction.

Figure 7. Flowchart showing different factors that influence the reaction mechanism of the replacement reaction and thus may change the activation energy for the process to take place.

Figure 8. Molar apatite-melt partition coefficient *D* versus the effective ionic radius of F, Cl and Br (Dong 2003).

Table 1. Solutions used in the hydrothermal experiments with various concentrations of Cl in solution.

Table 2. Experimental conditions for all four sets of experiments carried out to determine the influence of temperature, reaction time and Cl-concentration on the replacement of calcite powder and single crystals of calcite by apatite.

Table 3. Values for gradient *n* and rate constant *k* calculated for different temperatures and molarities.

Table 4. Activation energies calculated for reactions with different concentrations of Cl in solution. The deviations in E_a were calculated using the possible minimum and maximum value for y resulting from the errors in the Rietveld analyses.

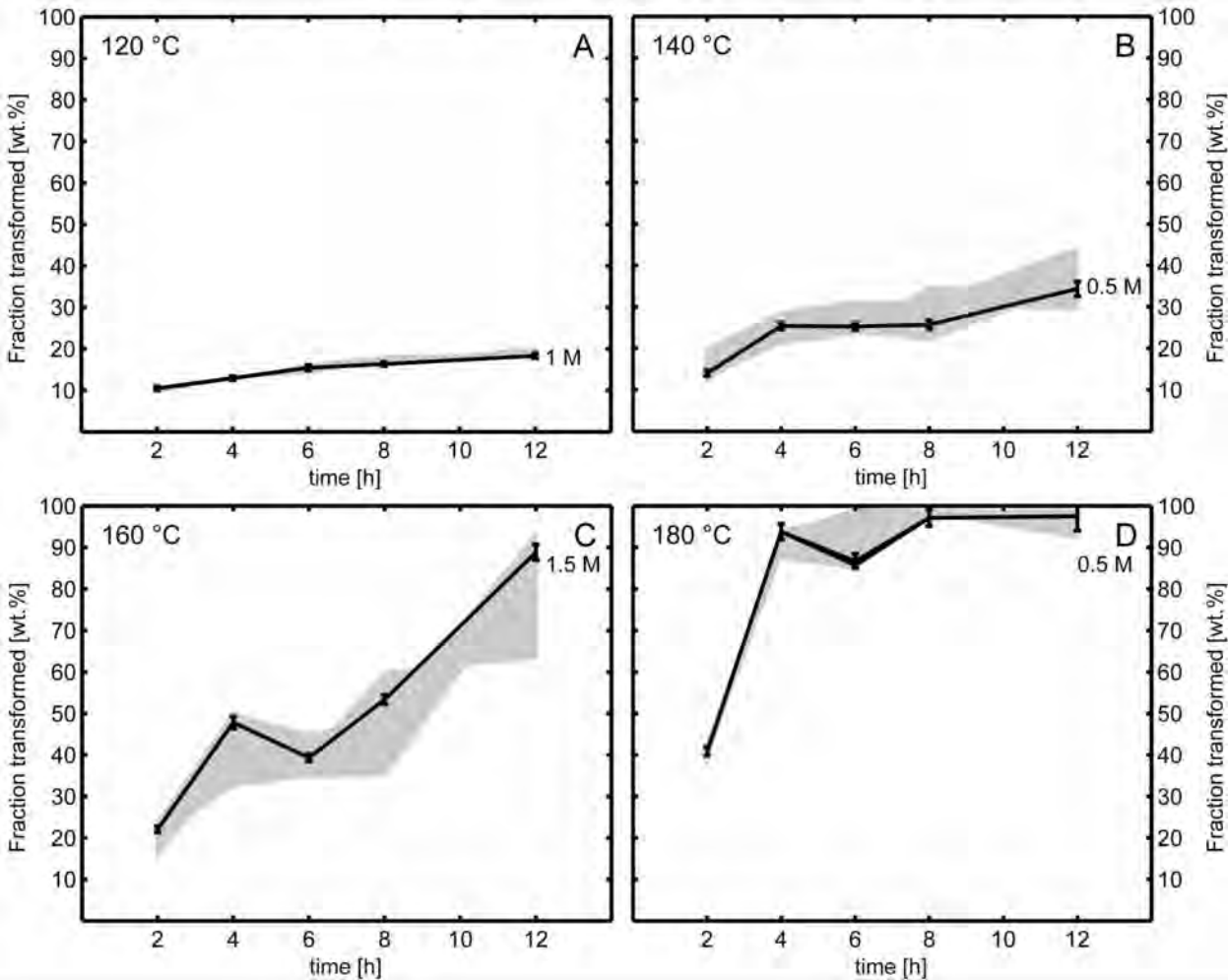
120 °C
A
1 M
140 °C
B
0.5 M
160 °C
C
1.5 M
180 °C
D
0.5 M
Fraction transformed [wt.%]
time [h]
100
90
80
70
60
50
40
30
20
10
2
4
6
8
10
12

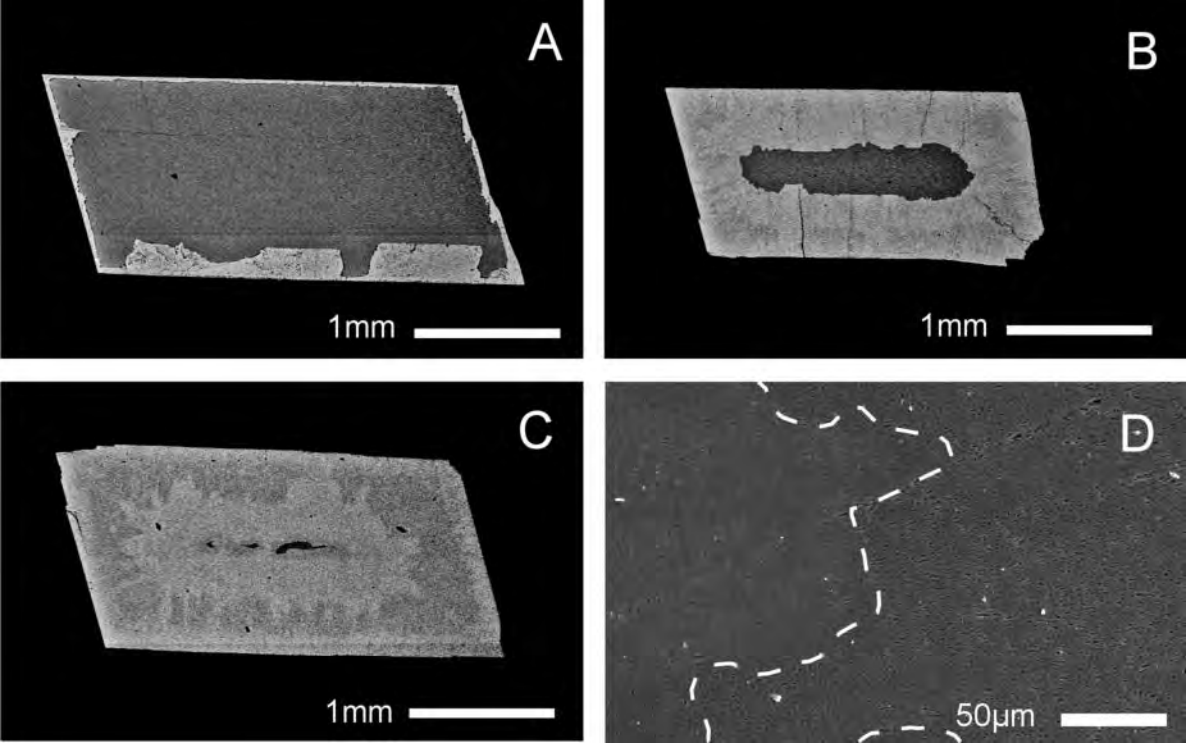
A
1mm
B
1mm
C
1mm
D
50μm

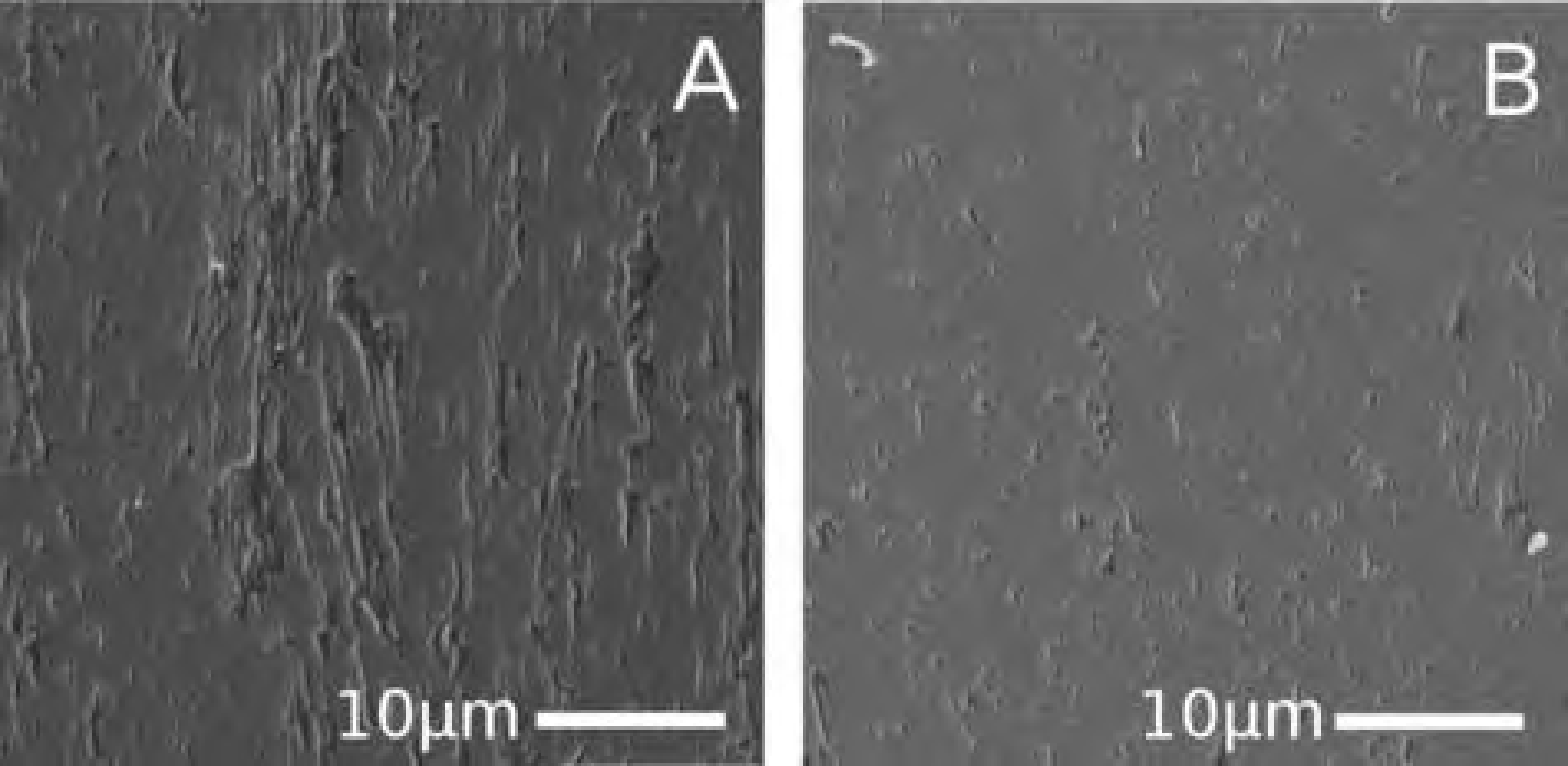
A
10μm
B
10μm

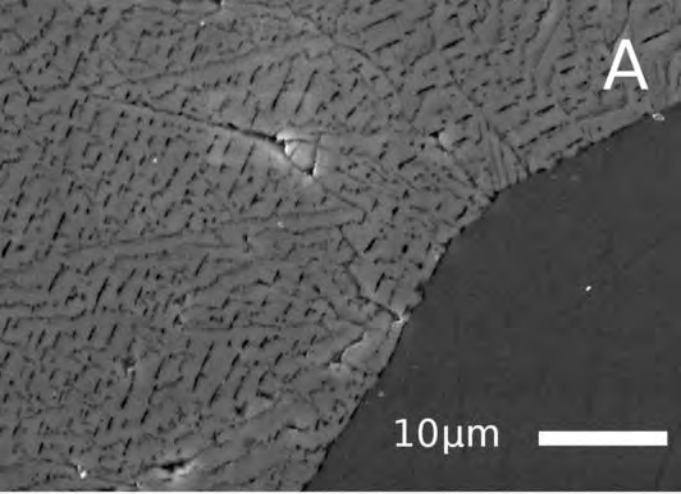
A
10µm

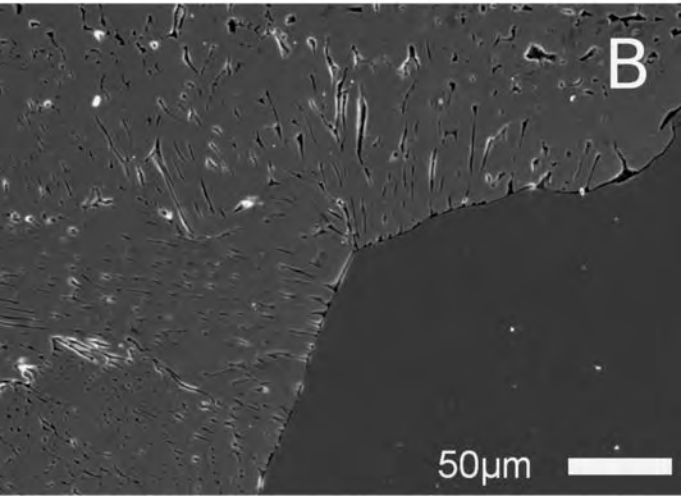
B
50µm

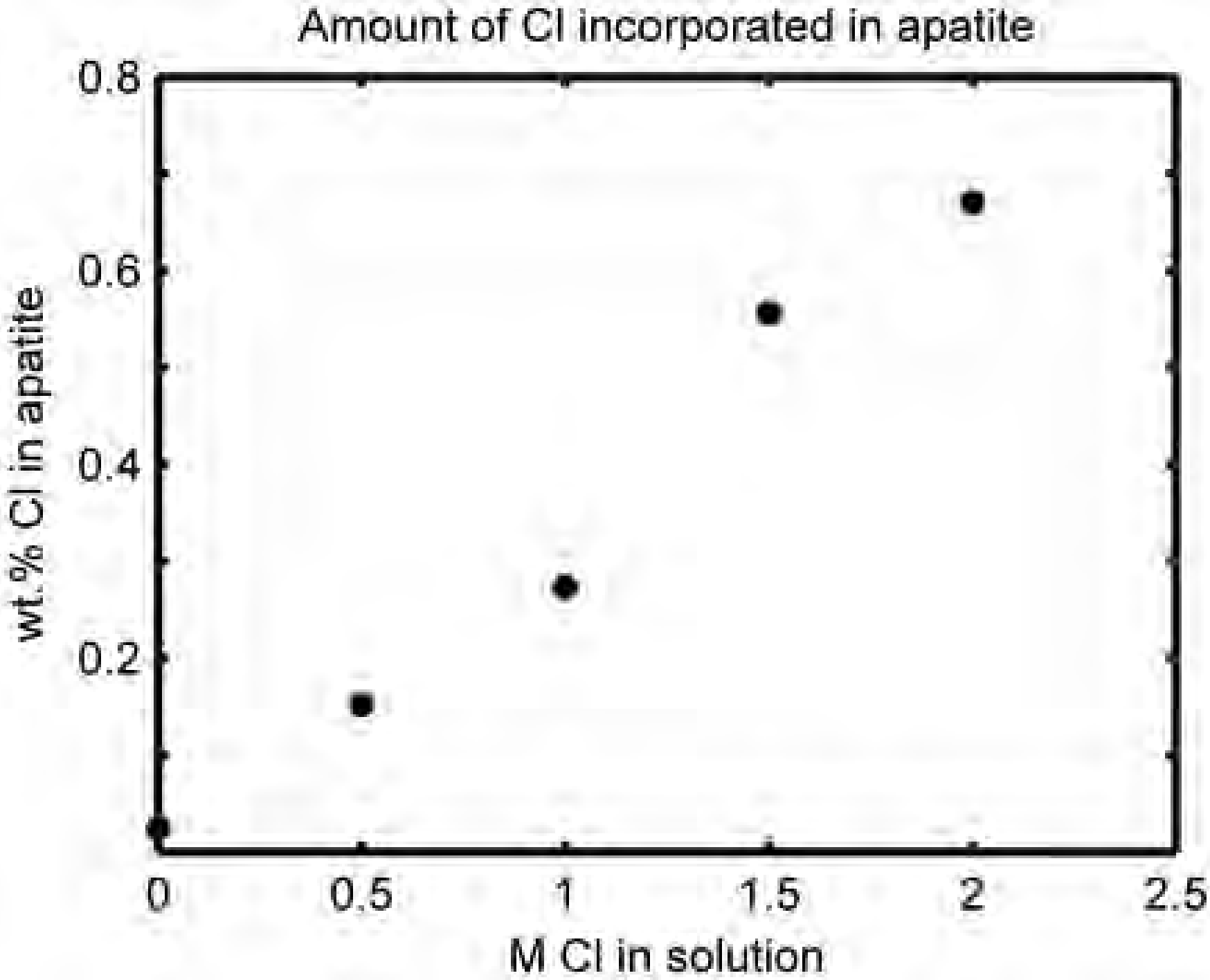
Amount of Cl incorporated in apatite
wt.% Cl in apatite
0.8
0.6
0.4
0.2
0
0.5
1
1.5
2
2.5
M Cl in solution

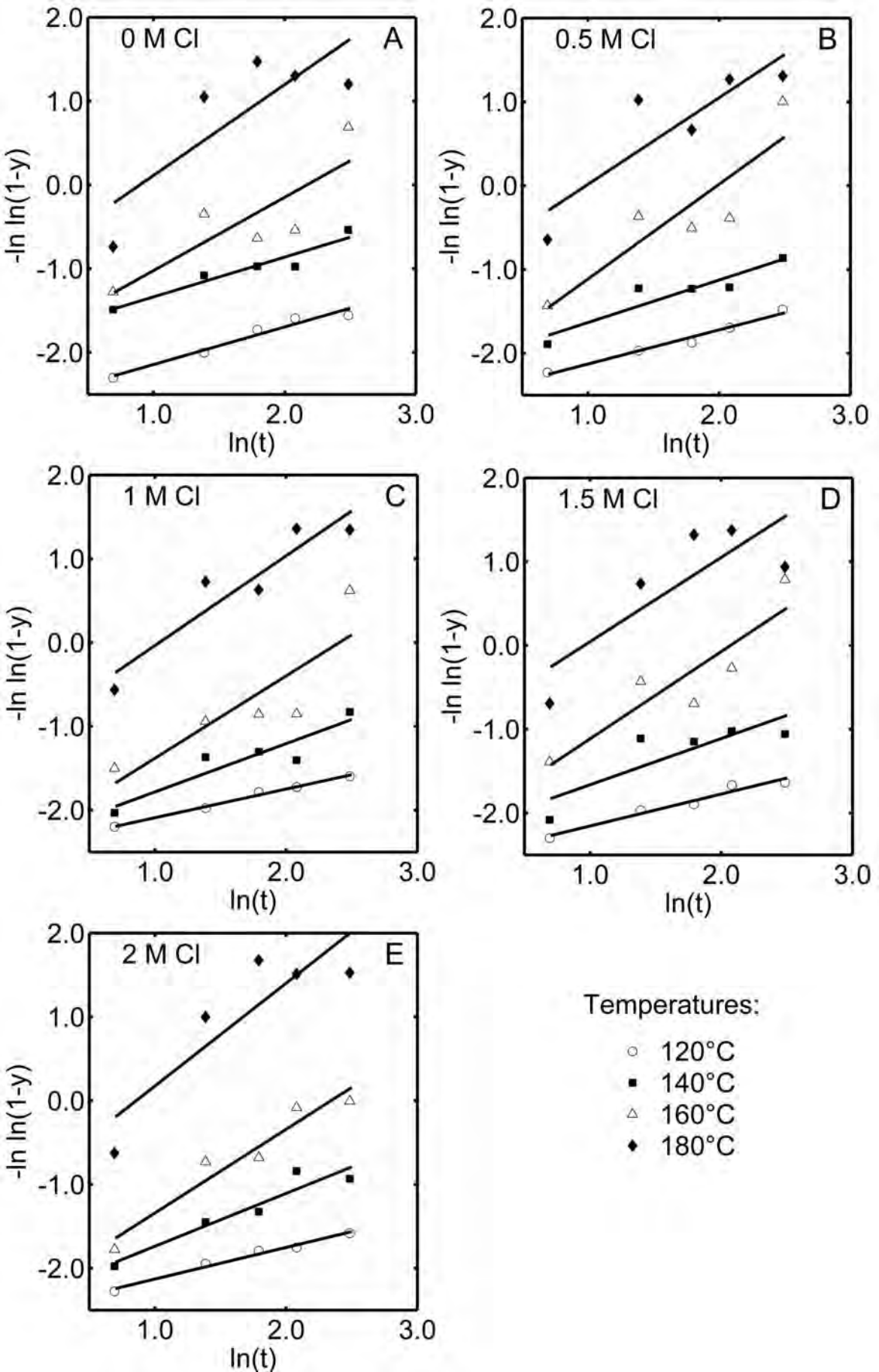
0 M Cl
A
0.5 M Cl
B
1 M Cl
C
1.5 M Cl
D
2 M Cl
E
-ln ln(1-y)
ln(t)
2.0
1.0
0.0
-1.0
-2.0
1.0
2.0
3.0
Temperatures:
120°C
140°C
160°C
180°C

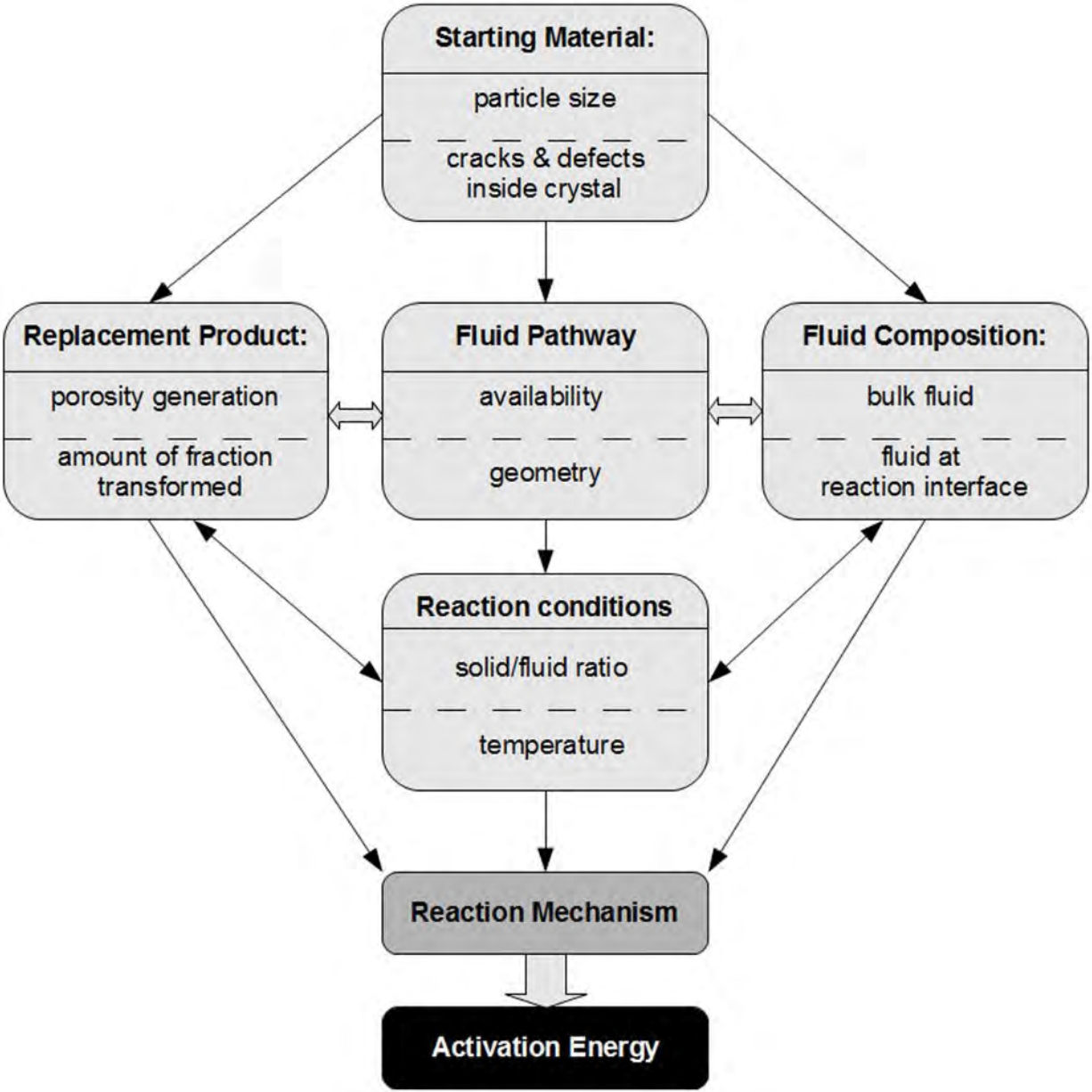
Starting Material:
particle size
cracks & defects inside crystal
Replacement Product:
porosity generation
amount of fraction transformed
Fluid Pathway
availability
geometry
Fluid Composition:
bulk fluid
fluid at reaction interface
Reaction conditions
solid/fluid ratio
temperature
Reaction Mechanism
Activation Energy

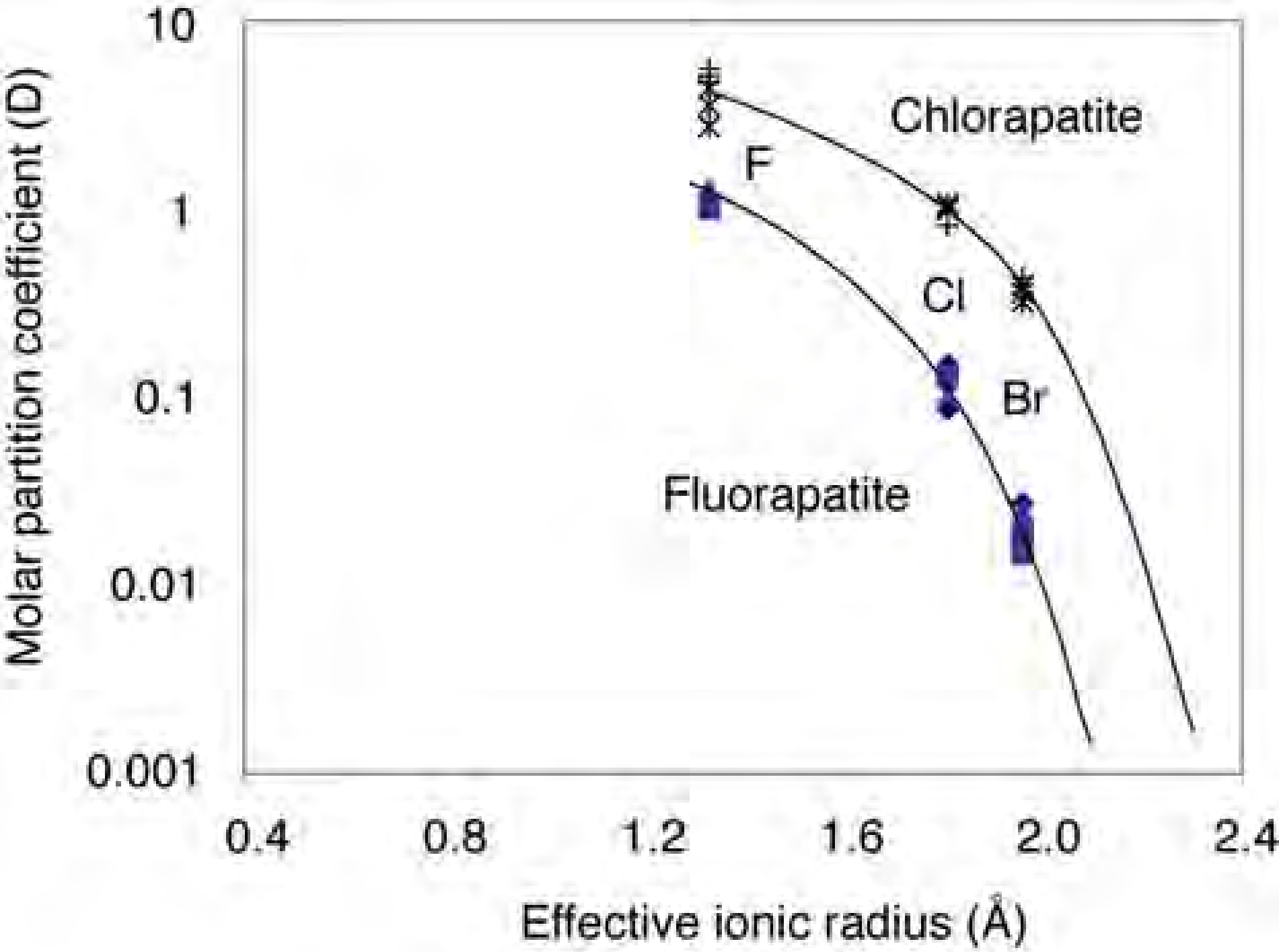
Molar partition coefficient (D)
10
1
0.1
0.01
0.001
0.4
0.8
1.2
1.6
2.0
2.4
Effective ionic radius (Å)
Chlorapatite
Fluorapatite
F
Cl
Br

$(NH_4)_2HPO_4$ [2.0 M]	NH_4Cl [2.0 M]	NH_4Cl [4.0 M]	H_2O (distilled)	M Cl	pH
1.0 ml	-	-	1.0 ml	0	8.06
1.0 ml	0.5 ml	-	0.5 ml	0.5	7.94
1.0 ml	1.0 ml	-	-	1.0	7.79
1.0 ml	-	0.75	0.25 ml	1.5	7.77
1.0 ml	-	1.0 ml	-	2.0	7.60

Starting material	Temperature [°C]	Time [h/days]	Cl-concentration [M]	Set
Calcite powder	120; 140; 160; 180	2h; 4h; 6h; 8h; 12h	0; 0.5; 1.0; 1.5; 2.0	1
Single calcite crystals	200	2 days	0; 0.5; 1.0; 1.5; 2.0	2
Single calcite crystals	200	1; 2; and 3 days	1.0	3
Single calcite crystals	140; 160	4 days	1.0	4

M Cl	*T* [°C]	*n*-value	*k*
0	120	0.449	0.003
	140	0.475	0.022
	160	0.875	0.114
	180	1.086	0.408
0.5	120	0.408	0.002
	140	0.508	0.015
	160	1.132	0.137
	180	1.035	0.373
1.0	120	0.342	0.001
	140	0.577	0.017
	160	0.983	0.09
	180	1.072	0.355
1.5	120	0.382	0.001
	140	0.552	0.018
	160	1.052	0.129
	180	1.006	0.384
2.0	120	0.377	0.001
	140	0.631	0.023
	160	0.999	0.096
	180	1.228	0.424

M Cl	E_a [kJ/mol]	Deviation	
		with y min.	with y max.
0	118.39	(-0.04)	(-0.42)
0.5	130.55	(1.25)	(-2.20)
1.0	145.23	(1.40)	(-1.85)
1.5	138.74	(-1.37)	(1.43)
2.0	136.77	(-0.53)	(-0.35)